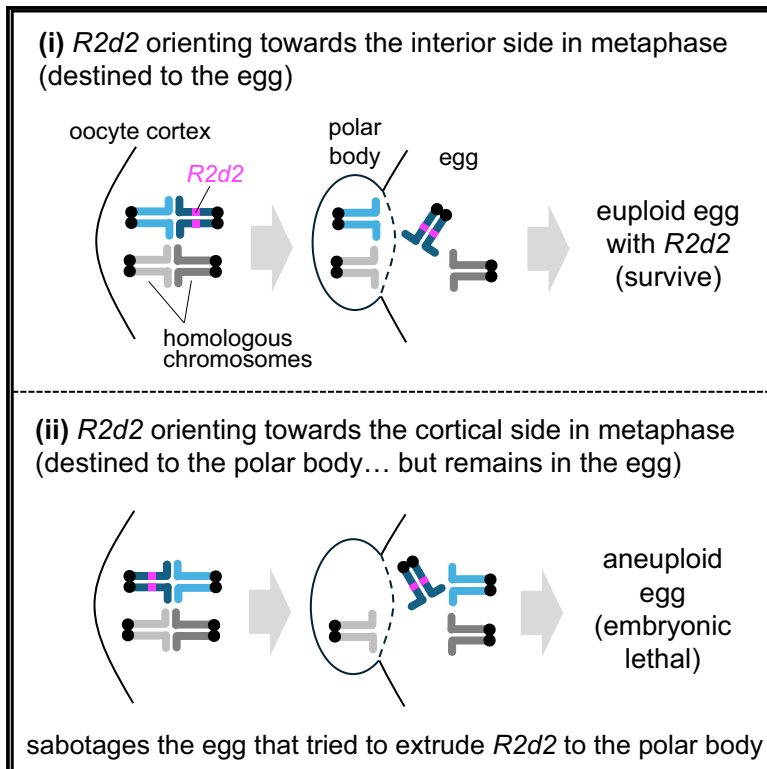


Current Biology

An egg-sabotaging mechanism drives non-Mendelian transmission in mice

Graphical abstract



Authors

Frances E. Clark, Naomi L. Greenberg, Duilio M.Z.A. Silva, ..., Leah F. Rosin, Michael A. Lampson, Takashi Akera

Correspondence

takashi.akera@nih.gov

In brief

Selfish elements cheat in meiosis to distort their transmission ratio, violating Mendel's law of segregation. Clark et al. show that a selfish element, *R2d2*, cheats in mouse oocytes by a hybrid mechanism, incorporating elements of both gamete killing and biased chromosome segregation.

Highlights

- First example of a meiotic driver using an egg-sabotaging mechanism in animals
- Meiotic driver, *R2d2*, induces egg aneuploidy, leading to embryonic lethality
- Egg-sabotaging mechanism explains both transmission bias and reduced fertility

Article

An egg-sabotaging mechanism drives non-Mendelian transmission in mice

Frances E. Clark,¹ Naomi L. Greenberg,¹ Duilio M.Z.A. Silva,¹ Emily Trimm,² Morgan Skinner,¹ R. Zaak Walton,¹ Leah F. Rosin,³ Michael A. Lampson,² and Takashi Akera^{1,4,5,*}

¹Cell and Developmental Biology Center, National Heart, Lung, and Blood Institute, National Institutes of Health, Bethesda, MD 20894, USA

²Department of Biology, School of Arts and Sciences, University of Pennsylvania, Philadelphia, PA 19104, USA

³Unit on Chromosome Dynamics, Division of Developmental Biology, Eunice Kennedy Shriver National Institute of Child Health and Human Development, National Institutes of Health, Bethesda, MD 20894, USA

⁴X (formerly Twitter): @TakashiAkeraLab

⁵Lead contact

*Correspondence: takashi.akera@nih.gov

<https://doi.org/10.1016/j.cub.2024.07.001>

SUMMARY

Selfish genetic elements drive in meiosis to distort their transmission ratio and increase their representation in gametes, violating Mendel's law of segregation. The two established paradigms for meiotic drive, gamete killing and biased segregation, are fundamentally different. In gamete killing, typically observed with male meiosis, selfish elements sabotage gametes that do not contain them. By contrast, killing is predetermined in female meiosis, and selfish elements bias their segregation to the single surviving gamete (i.e., the egg in animal meiosis). Here, we show that a selfish element on mouse chromosome 2, *Responder to drive 2* (*R2d2*), drives using a hybrid mechanism in female meiosis, incorporating elements of both killing and biased segregation. We propose that if *R2d2* is destined for the polar body, it manipulates segregation to sabotage the egg by causing aneuploidy, which is subsequently lethal in the embryo, ensuring that surviving progeny preferentially contain *R2d2*. In heterozygous females, *R2d2* orients randomly on the metaphase spindle but lags during anaphase and preferentially remains in the egg, regardless of its initial orientation. Thus, the egg genotype is either euploid with *R2d2* or aneuploid with both homologs of chromosome 2, with only the former generating viable embryos. Consistent with this model, *R2d2* heterozygous females produce eggs with increased aneuploidy for chromosome 2, increased embryonic lethality, and increased transmission of *R2d2*. In contrast to typical gamete killing of sisters produced as daughter cells in a single meiosis, *R2d2* prevents production of any viable gametes from meiotic divisions in which it should have been excluded from the egg.

INTRODUCTION

Mendel's law of segregation states that alleles segregate randomly during meiosis, transmitting to gametes with an equal (50%) chance. However, some genetic elements violate this law to preferentially transmit to the next generation, with associated fitness costs to the host (e.g., reduced fertility).^{1–7} Such selfish elements that cheat during meiosis are called meiotic drivers, and distinct mechanisms to achieve their biased transmission have been identified in several species.⁸ These drive mechanisms generally fall into one of two categories, preferential segregation or gamete killing.⁴ Female meiotic drive is thought to be accomplished primarily through preferential segregation to the egg, exploiting the inherent asymmetry in female meiosis: each division produces one smaller cell (polar body) and one larger cell (egg), and only the chromosomes that segregate to the egg will transmit.^{3,9–11} By contrast, male meiosis undergoes symmetric divisions, and cheating mostly happens post meiosis, typically through killer meiotic drive.^{5,7,8} Killer meiotic drivers act through the sabotage or death of competitor gametes (sperm or

spores) that do not carry them.^{5,7,12} Although disabling non-carrier sperm often reduces fertility, sperm killer systems allow more eggs to be fertilized by sperm that carry meiotic drivers, leading to biased transmission to the offspring.¹³

The asymmetry of female meiosis allows meiotic drivers to increase transmission by manipulating chromosome segregation to remain in the egg. Centromeres have an ideal opportunity to cheat in female meiosis because they interact with the spindle to direct chromosome orientation and segregation.^{14–19} Indeed, selfish expanded centromeres preferentially remain in the egg in both animals and plants.^{20–22} Selfish mouse centromeres have been the primary system to study cell biological mechanisms underlying meiotic drive in animal female meiosis.^{21,23–25} Other loci usually do not control chromosome-spindle interactions and, therefore, it is unknown how non-centromeric meiotic drivers manipulate their segregation patterns, except for maize knob that exploit an asymmetry specific to plant female meiosis.^{3,26–28} We chose the selfish *Responder to drive 2* (*R2d2*) locus as a model system to tackle this question in an animal system. *R2d2* is a repetitive DNA of a 127-kb-long monomer found on

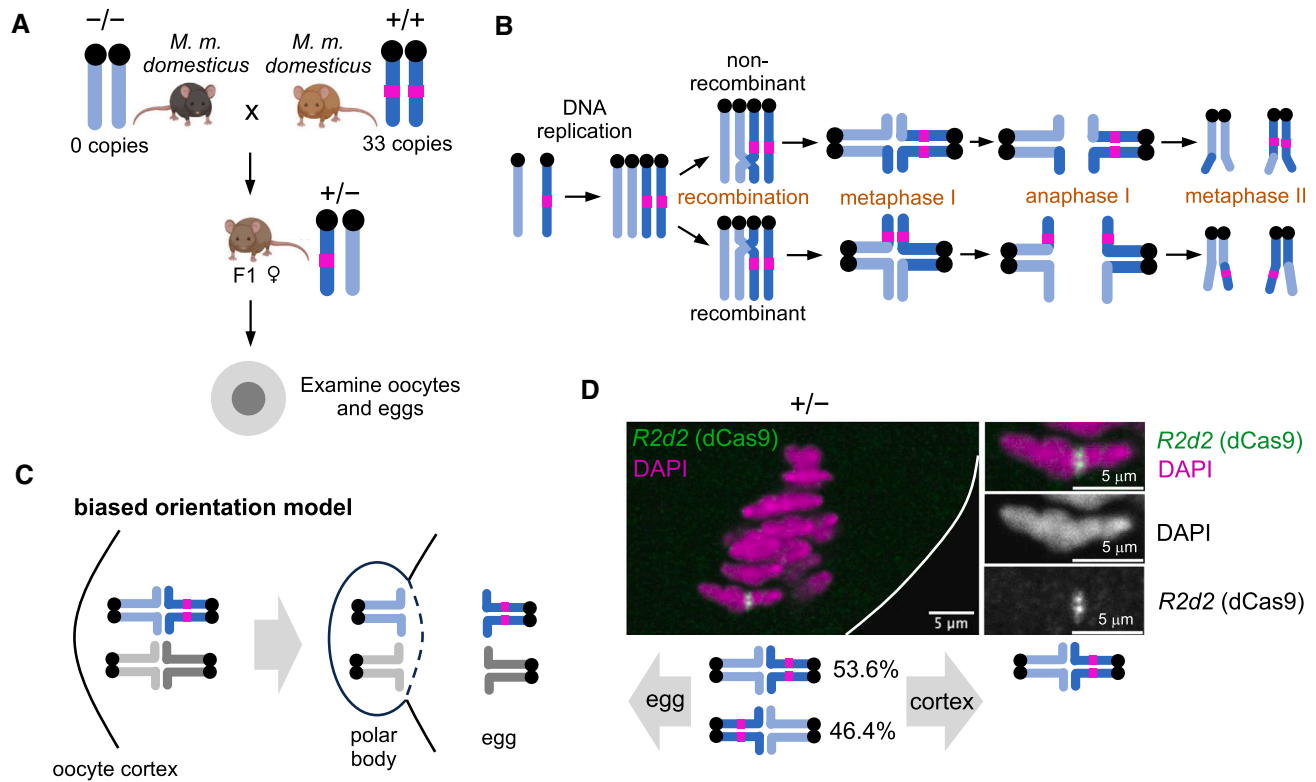


Figure 1. *R2d2* randomly orients on the metaphase I spindle in female meiosis

(A) Female F1 hybrids between two *M. m. domesticus* strains with different *R2d2* copy numbers (*R2d2* heterozygous mice, +/-) as experimental systems to study meiotic drive of *R2d2*. Oocytes and eggs collected from +/- mice (C57BL/6J x WSB/EiJ²⁹ and BXD19/TyJ x WSB/EiJ hybrids) and -/- mice (the CF1 strain) were used throughout this study, unless specified in the figure legend (see STAR Methods, mouse strains).

(B) Schematic showing recombinant and non-recombinant chromosomes, depending on whether there is crossover between *R2d2* and the centromere. Non-recombinants can cheat in meiosis I whereas recombinants can cheat in meiosis II.

(C) Schematic showing the biased orientation model for *R2d2* meiotic drive.

(D) *R2d2* heterozygous (+/-) oocytes expressing dCas9-EGFP and gRNA targeting the *R2d2* sequence were fixed shortly before anaphase I and stained for EGFP. The fraction of oocytes with the *R2d2* locus oriented toward either the egg or cortical pole was measured; *n* = 39 cells. White line, oocyte cortex. Note that we focused only on non-recombinant chromosomes, which can cheat in meiosis I.

See also Figure S1 and Data S1.

mouse chromosome 2 and experiences transmission rates above 95% from heterozygous female mice.^{29–31} Transmission from heterozygous male mice is Mendelian (i.e., 50%).²⁹ The female meiotic drive is associated with a fertility cost of ~30% reduction in litter size due to embryonic lethality.²⁹ The molecular mechanisms underlying biased transmission and embryonic lethality are completely unknown.

RESULTS

Cell biological approaches to investigate *R2d2* meiotic drive

R2d2 is located in the middle of a telocentric chromosome (i.e., Ch.2: 83,790,939–84,701,151 in the GRCm38/mm10 mouse reference assembly, where chromosome 2 represents 182 Mb).²⁹ This locus is a duplication of *R2d1*, present ~6 Mb away on the same chromosome (Figure S1A).³⁰ After the initial duplication event that occurred between 2 and 3.5 million years ago, the *R2d2* locus expanded, resulting in a repetitive tandem arrayed element. Consequently, some mouse strains in the

Mus genus completely lack *R2d2*, some possess a single copy of the *R2d2* monomer, and others have several copies of *R2d2* tandemly repeated (e.g., the WSB/EiJ strain is homozygous for 33 copies of the *R2d2* monomer).²⁹

As an experimental system to study *R2d2* meiotic drive, we used *Mus musculus domesticus* intra-subspecific hybrid female mice heterozygous for the *R2d2* locus, which were previously shown to exhibit biased transmission (Figure 1A, +/-).²⁹ We developed two complementary methods to visualize the *R2d2* locus in mouse oocytes: CRISPR-Cas9-based labeling using dCas9-EGFP plus guide RNA (gRNA) targeting the *R2d2* DNA sequence and Oligopaint fluorescence *in situ* hybridization (FISH) (Figures S1B–S1E; see STAR Methods).^{32,33} Oligopaint FISH shows more robust labeling than dCas9-EGFP in fixed oocytes, while dCas9-EGFP is compatible with both fixed and live cell imaging.

In female meiosis, both divisions produce a polar body, and female meiotic drive can occur in either of the two meiotic divisions, depending on when the driving locus segregates from its homolog.²⁶ Homologous centromeres segregate in meiosis

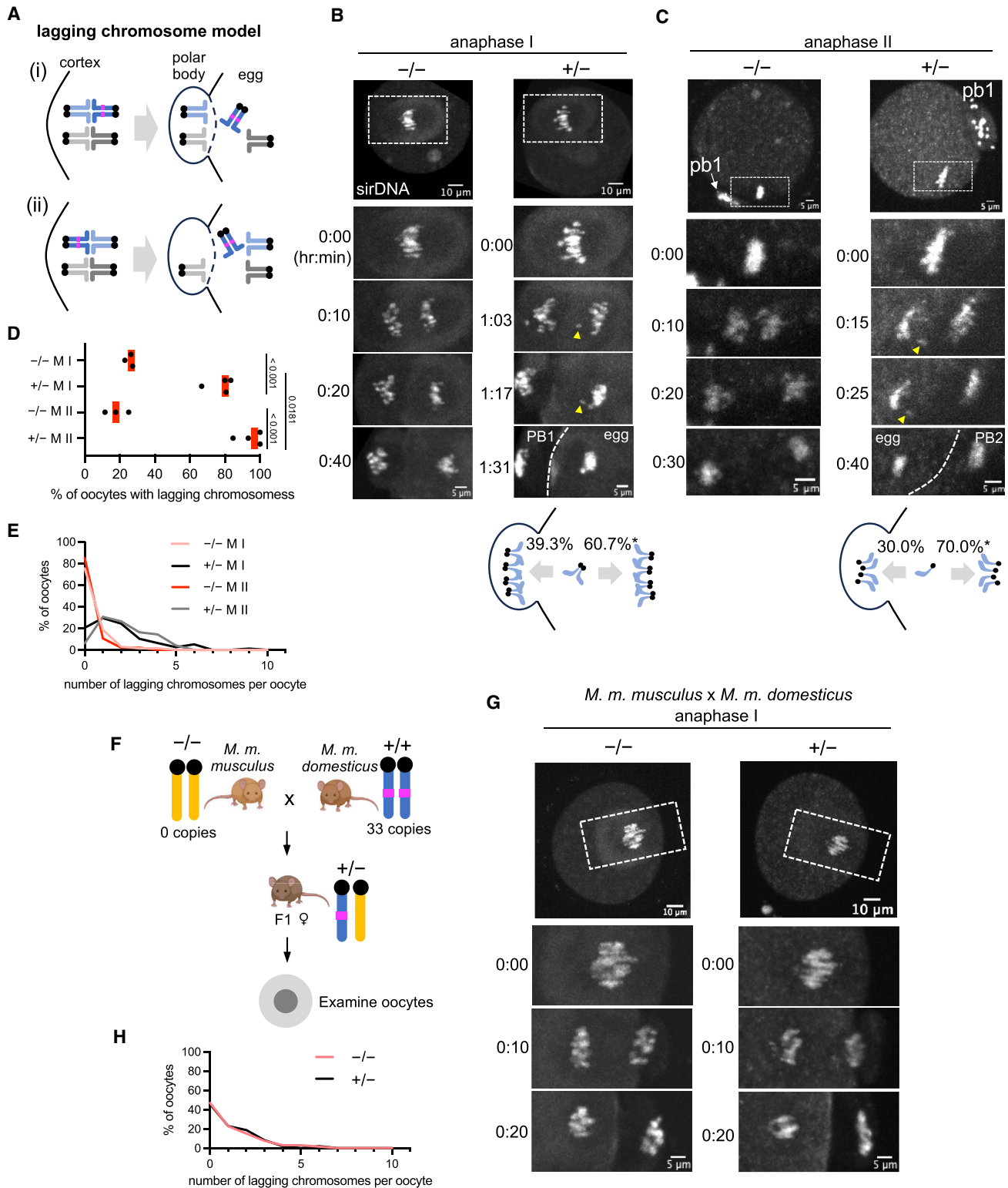


Figure 2. *R2d2* meiotic drive is associated with increased anaphase lagging

(A) Schematic showing the anaphase lagging model for *R2d2* meiotic drive.

(B and C) Control ($-/-$) and *R2d2* heterozygous ($+/-$) meiosis I oocytes (B) and meiosis II eggs (C) were stained with sirDNA to visualize chromosomes and imaged live at anaphase ($n = 65$ and 80 meiosis I oocytes for control and *R2d2* heterozygote, respectively, and $n = 47$ and 49 meiosis II eggs for control and *R2d2* heterozygote, respectively). Note that the lagging chromosomes (yellow arrowheads) eventually remained in the egg. The segregation pattern of lagging

(legend continued on next page)

I and, therefore, selfish centromeres cheat exclusively in meiosis I.³⁴ By contrast, a non-centromeric locus like *R2d2* can cheat either in meiosis I or II, depending on the crossover position (Figure 1B).^{27,35} If the crossover is not located between *R2d2* and the centromere (non-recombinant), one pair of sister chromatids has *R2d2* and the other pair does not (Figure 1B, top). In this case, the *R2d2* locus segregates from its homolog in meiosis I, and the cheating could happen in meiosis I, as with centromeres. Alternatively, crossover between the centromere and *R2d2* will create recombinant chromatids, where one sister chromatid of each pair has *R2d2* and the other sister does not (Figure 1B, bottom). In this configuration, both products of meiosis I receive one chromatid with *R2d2*, so there is no opportunity for cheating in meiosis I. *R2d2* segregates from its homolog in meiosis II, providing the opportunity to bias its segregation to the egg. Given *R2d2*'s central location within the chromosome, it could, in principle, cheat in either meiosis I or meiosis II, depending on the crossover position.

***R2d2* randomly orients on the metaphase I spindle in female meiosis**

In metaphase I in mouse oocytes, the spindle assumes a position perpendicular to the cell membrane, with one pole facing the oocyte cortex and the other facing the interior of the cell.³⁶ Selfish centromeres preferentially orient toward the interior side of the metaphase I spindle to preferentially remain in the egg.^{20,21} Depending on the crossover position, *R2d2* could cheat by this mechanism in either metaphase I (non-recombinant) or metaphase II (recombinant). We tested for biased orientation in metaphase I (Figure 1C), when the spindle is positioned perpendicular and we can determine which spindle pole will be extruded to the polar body and which will be retained in the egg.³⁶ By contrast, the spindle is parallel to the cortex at metaphase II, so we cannot predict which pole will be extruded to the polar body.^{37,38} Using dCas9-EGFP to visualize *R2d2*, we did not find a significant orientation bias of non-recombinant chromosomes in metaphase I (Figure 1D). Based on this finding, it is unlikely that *R2d2* biases its transmission by biased orientation on the spindle, indicating that *R2d2* and centromeres use distinct cheating strategies.

Anaphase lagging model for meiotic drive

Another possible cheating mechanism for *R2d2* that is compatible with both meiosis I and II is to induce its own chromosome to lag in anaphase, without affecting anaphase movement of the paired chromosome 2 lacking *R2d2*. Because of the highly asymmetric cell division in female meiosis, it is reasonable to suggest that lagging chromosomes might be carried with the

larger amount of cytoplasm into the egg (Figure 2A). If *R2d2* initially orients toward the interior side of the meiosis I spindle, it lags and still ends up in the egg, with the homologous chromosome 2 in the polar body (Figure 2Ai). If *R2d2* initially orients toward the cortex, it lags and remains in the egg along with the homologous chromosome 2, causing aneuploidy of chromosome 2 and subsequent embryonic lethality (Figure 2Aii).^{39,40} Similar mechanisms can be applied to meiosis II, where recombinant sister chromatids with and without *R2d2* compete for segregation to the egg. This embryo killing strategy leads to biased transmission of *R2d2* because surviving embryos are euploid with *R2d2*.

The anaphase lagging model makes several predictions that can be experimentally tested: (1) lagging chromosomes should be present at high frequency in crosses where cheating occurs, (2) lagging chromosomes preferentially end up in the egg rather than the polar body, (3) chromosome 2 with *R2d2* lags more frequently than other chromosomes, and (4) aneuploidy for chromosome 2 is more frequent than for other chromosomes in crosses where cheating occurs. Although these predictions apply to both meiosis I and meiosis II, depending on the crossover position, we focused primarily on meiosis I because of technical difficulty in efficiently labeling *R2d2* in anaphase II.

We tested the first and second predictions by live imaging of *R2d2* heterozygous oocytes and control oocytes without *R2d2*. Heterozygous oocytes had significantly more lagging chromosome events in anaphase I and II compared with controls (Figures 2B–E). Furthermore, these lagging chromosomes preferentially remained in the egg (Figures 2B and 2C). To test whether anaphase lagging is functionally related to preferential transmission, we examined a hybrid that is heterozygous for *R2d2* but does not exhibit meiotic drive. Previous studies have revealed that the strength of *R2d2* drive differs depending on the strains involved (reporting transmission ratios ranging from 50% to 95%), which suggests that other, unlinked loci modify the strength of drive.²⁹ For example, no drive was observed when the same *M. m. domesticus* strain with expanded *R2d2*, used in our previous experiments, was crossed with a *M. m. musculus* strain (Figure 2F). To control for any chromosomal lagging issues introduced by an inter-subspecific hybridization, we compared this non-driving hybrid with a control *M. m. musculus* × *M. m. domesticus* hybrid lacking *R2d2*. Oocytes from the non-driving hybrid containing *R2d2* did not show an increased anaphase lagging rate compared with the control hybrid without *R2d2* (Figures 2G and 2H). In addition to the non-driving hybrid, we also analyzed a weakly driving hybrid (~67% transmission bias) and found intermediate frequencies of anaphase lagging

chromosomes was quantified; chi-squared test for goodness of fit was used to examine the deviation from the expected 50:50 ratio (B, $n = 145$ lagging chromosomes from 76 meiosis I oocytes, $^*p = 0.01004$; C, $n = 40$ lagging chromosomes from 17 meiosis II eggs, $^*p = 0.01141$).

(D and E) Based on the live imaging data in (B) and (C), the fraction of oocytes with at least one lagging chromosome (D, each dot represents an independent experiment; red line, mean; unpaired two-tailed t test was performed, only significant p values are shown) and the distribution of the number of lagging chromosomes per oocyte were quantified.

(F) Female F1 hybrids between a *M. m. domesticus* strain with expanded *R2d2* (WSB/EiJ) and a *M. m. musculus* strain without it (PWD/PhJ) show Mendelian segregation of *R2d2*.

(G and H) Control (–/–, PWD/PhJ × C57BL/6J) and *R2d2* heterozygous (+/–, PWD/PhJ × WSB/EiJ) oocytes in the *M. m. musculus* × *M. m. domesticus* hybrid genetic background were stained with sirDNA to visualize chromosomes and imaged live at anaphase I (G), and the distribution of the number of lagging chromosomes per oocyte was quantified (H, $n = 66$ and 48 oocytes for control and *R2d2* heterozygote, respectively).

See also Figure S2.

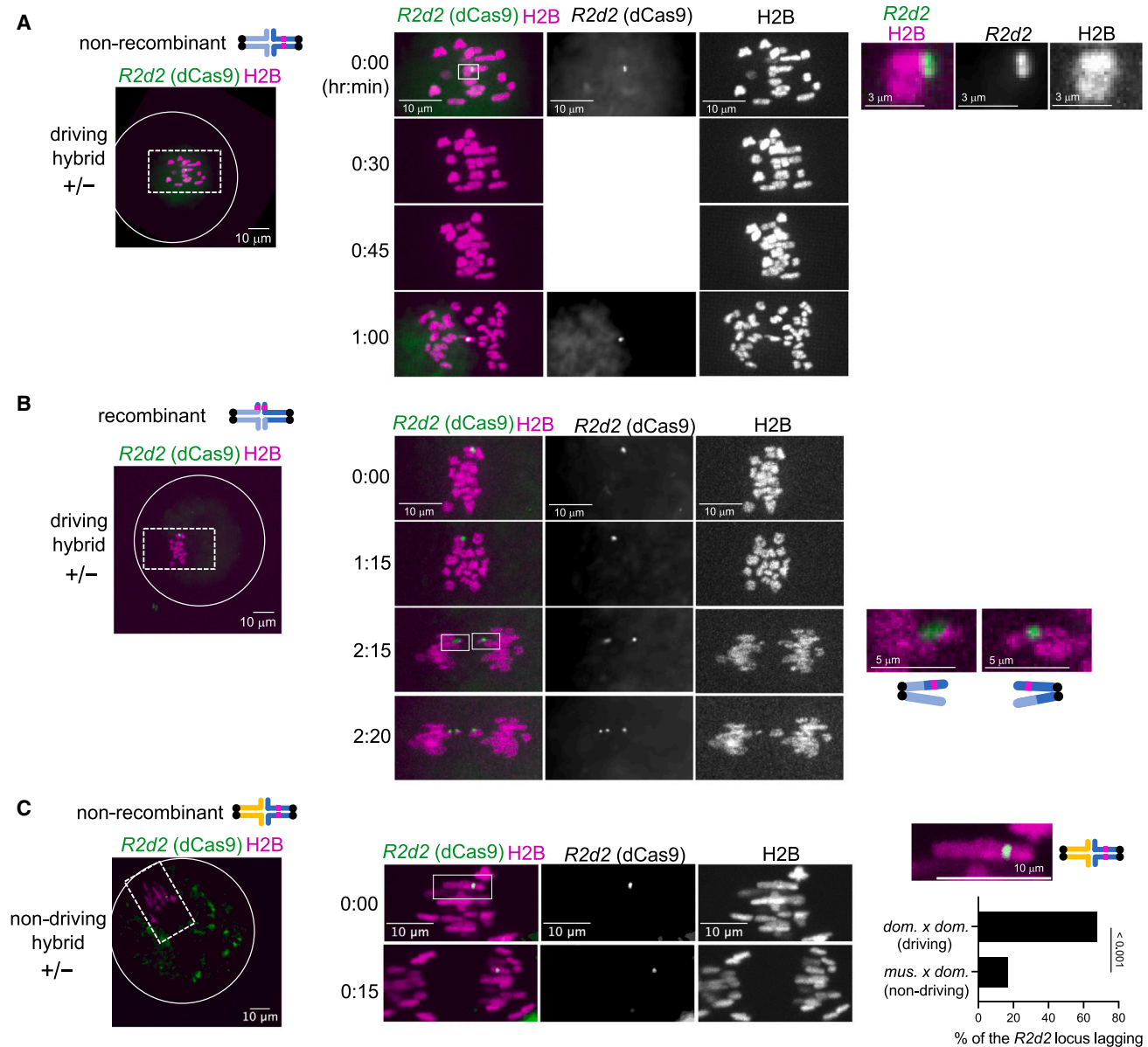


Figure 3. *R2d2* induces its own chromosome to lag in anaphase

R2d2 heterozygous (+/–) oocytes expressing histone H2B-mCherry (chromosomes), dCas9-EGFP, and gRNA targeting the *R2d2* DNA sequence were imaged live at anaphase I; white line, oocyte cortex; $n = 35$ and 18 cells for driving (A and B) and non-driving (C) hybrids, respectively. For the non-recombinant chromosome example (A), we imaged the dCas9-EGFP signals only at the first time point and at the anaphase onset to minimize photobleaching and phototoxicity. In the recombinant chromosome example (B), three dCas9 signals were observed at the 2 h 20 min time point due to the splitting of the *R2d2* locus on one of the homologs (see also Figure S3A). The fraction of oocytes with the dCas9 signal lagging in anaphase I was quantified; chi-squared test of independence was used to calculate the p values in the graph. We used the Denoise.ai software (Nikon) to reduce noise and follow the *R2d2* locus better in anaphase I. See also Figure S3.

(Figure S2, A/J \times WSB/EiJ),²⁹ demonstrating a correlation between anaphase lagging frequencies and drive strength. Together, these observations are consistent with the first two predictions of the anaphase lagging model for biased transmission of *R2d2*.

To test the third prediction, that chromosome 2 with *R2d2* lags more frequently than other chromosomes, we visualized *R2d2* in anaphase I using dCas9-EGFP. We found that 63.9% of heterozygous oocytes experienced chromosome 2 with *R2d2* lagging

in anaphase I, while other chromosomes segregated to the spindle poles (Figure 3). In some oocytes, we were able to distinguish between recombinant and non-recombinant chromosomes and found anaphase I lagging in both cases (Figures 3A and 3B). Only non-recombinant chromosomes can cheat in meiosis I, but most of the recombinant chromosomes appear to eventually segregate equally in meiosis I, allowing them to cheat in meiosis II (see below).

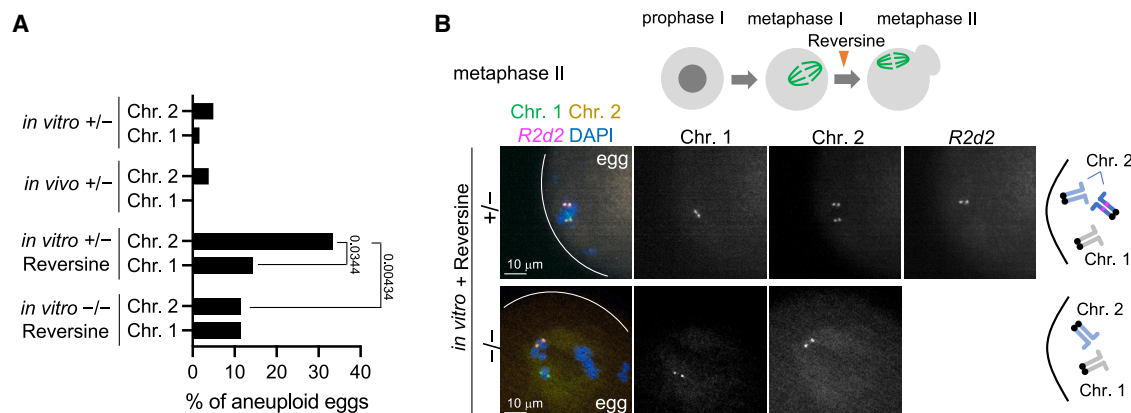


Figure 4. Chromosome 2 with *R2d2* has a higher aneuploid rate

(A) Quantification of the fraction of the oocytes that are aneuploid for chromosome 1 or 2 at the metaphase II stage ($n = 52, 52, 84, 35, 162, 61, 78,$ and 36 oocytes for *in vitro* $-/-$ reversine Chr. 2, *in vitro* $-/-$ reversine Chr. 1, *in vitro* $+/-$ reversine Chr. 2, *in vitro* $+/-$ reversine Chr. 1, *in vitro* $+/-$ Chr. 2, *in vitro* $+/-$ Chr. 1, *in vivo* $+/-$ Chr. 2, and *in vivo* $+/-$ Chr. 1; chi-squared test of independence was used to calculate the p values in the graph, only significant p values are shown). (B) Top schematic shows the reversine treatment of mouse oocytes at metaphase I. Control ($-/-$) and *R2d2* heterozygous ($+/-$) oocytes were matured *in vitro* in the presence of reversine and fixed at metaphase II to visualize chromosome 1 and 2 and the *R2d2* locus with Oligopaint FISH. White lines, egg cell cortex. See also Figure S4.

To further interrogate whether the lagging of chromosome 2 with *R2d2* is indeed associated with drive, rather than an unintended artifact of the dCas9-EGFP system, we visualized *R2d2* with dCas9-EGFP in heterozygous oocytes from the non-driving hybrid. Chromosome 2 with *R2d2* had a lower incidence of lagging in the non-driving hybrid compared with the driving hybrid (Figures 2F and 3C). These findings are consistent with the third model prediction and suggest that *R2d2* can induce its own chromosome to lag in anaphase as a mechanism to bias its transmission to surviving progeny.

To induce lagging, *R2d2* may interact with some intracellular structure to slow its poleward movement during anaphase. If the centromere of chromosome 2 is pulled toward the spindle pole but the *R2d2* locus is resisting poleward movement, the *R2d2* locus should experience tension due to the tug-of-war. Consistent with this idea, we often observed splitting and stretching of the *R2d2* locus in anaphase I in oocytes from the driving hybrid, but not in oocytes from the non-driving hybrid (Figures S3A and S3B). As a possible alternative explanation for anaphase I lagging, bivalents containing *R2d2* might fail to resolve into univalents. Live imaging of centromeres in *R2d2* heterozygous oocytes (Figure S3C) revealed that 96.8% of the anaphase lagging chromosomes separated properly into univalent chromosomes, arguing against this possibility.

To test the fourth prediction regarding the higher aneuploidy for chromosome 2 with *R2d2*, we measured aneuploidy in metaphase II eggs using Oligopaint FISH (Figures 4A and 4B). Although the overall aneuploidy rates were low, chromosome 2 with *R2d2* appeared to have higher aneuploidy rates than chromosome 1, which has a similar size (Figure 4A, *in vitro* $+/-$ and *in vivo* $+/-$). The low chromosome 2 aneuploidy rate by metaphase II suggests that meiotic drive by anaphase lagging is weaker in meiosis I compared with meiosis II. Indeed, our results show that frequencies of lagging chromosome events and lagging chromosomes remaining in the egg are both higher in meiosis II compared with meiosis I (Figures 2B–2D). A high

transmission rate would therefore depend on recombinant chromosomes cheating in meiosis II. We find by Oligopaint FISH analyses that 77.5% of metaphase II eggs contained recombinant chromatids (Figure S4A), consistent with *R2d2* cheating more often in meiosis II compared with meiosis I. Even though recombinant chromosomes lag in anaphase I (Figure 3B), they eventually segregate equally in most cases, providing the opportunity for them to cheat in meiosis II.

Because of the large number of animals required to compare low aneuploidy rates, we sensitized the system by inhibiting a spindle checkpoint kinase, MPS1, with the inhibitor reversine to increase the basal aneuploidy levels. We collected prophase I oocytes from *R2d2* heterozygous mice, treated with reversine at metaphase I, and matured them *in vitro* until metaphase II (Figure 4B). Reversine-treated eggs confirmed our finding that chromosome 2 with *R2d2* has a higher aneuploidy rate than chromosome 1 (Figures 4A and 4B). To test whether the presence of *R2d2* is involved in the higher aneuploidy rate of chromosome 2, oocytes from wild-type ($-/-$) mice were matured to metaphase II *in vitro* in the presence of reversine. The aneuploidy rate of chromosome 2 without *R2d2* was similar to that of chromosome 1 and significantly less compared with chromosome 2 with *R2d2* (Figures 4A and 4B). Collectively, these results are consistent with our anaphase lagging model where *R2d2* can increase chromosome 2 aneuploidy via lagging to bias its transmission (Figure 2A).

DISCUSSION

R2d2 sabotages the egg with the “wrong” genotype to bias its transmission

The anaphase lagging model incorporates elements of both biased segregation and killer meiotic drive systems. The former typically manipulates segregation to preferentially remain in the egg, without creating aneuploidy.^{3,41,42} *R2d2* also manipulates segregation, but by lagging in anaphase to escape segregating

to the polar body, resulting in aneuploidy. Killer meiotic drivers typically act through sabotage of competitor gametes that do not carry the driver.^{43–46} Similarly, the aneuploidy induced by *R2d2* lagging is expected to lead to embryonic lethality, but of embryos that inherited both alleles. This mechanism does not increase the absolute number of euploid eggs possessing *R2d2* but instead enriches *R2d2* among surviving euploid offspring. This model is consistent with two previous findings.^{29,47} First, stronger *R2d2* meiotic drive is associated with higher embryonic lethality rates as a fitness cost. Second, *R2d2* biases its transmission rate, mainly by decreasing the absolute number of wild-type progeny without *R2d2* rather than by increasing the number of progenies with *R2d2*. Therefore, the anaphase lagging model can explain the mechanisms underlying both the biased transmission and the fitness cost associated with *R2d2* meiotic drive. This work provides cell biological insights into how non-centromeric loci can bias their transmission through female meiosis and raises two important questions. First, how does *R2d2* induce anaphase lagging? Second, how do lagging chromosomes remain in the egg?

How does *R2d2* induce anaphase lagging and remain in the egg?

In some plants, accessory B chromosomes induce anaphase lagging by preventing chromosome separation and bias their segregation during pollen mitosis.^{48–50} By contrast, we propose that chromosomes carrying *R2d2* separate appropriately, but the *R2d2* locus interacts with some intracellular structure (e.g., the spindle) to maintain its position during anaphase and induce lagging. This model is consistent with the observations that chromosomes separate normally in anaphase (Figure S3C) and that the *R2d2* locus appears to be under tension in anaphase more often in driving hybrids than non-driving hybrids (Figures S3A and S3B). One possibility is that *R2d2* interacts with the spindle using microtubule-binding proteins, as seen with maize knob domains, which recruit kinesin-14 motor proteins.^{27,28} Alternatively, *R2d2* may interact with a different cellular structure, such as the actin network or endomembranes surrounding the oocyte spindle.^{51–53}

We found that anaphase lagging chromosomes preferentially segregated to the egg in both meiosis I and II (Figures 2B and 2C). This preferential retention may be specific to the mechanism of *R2d2* lagging. For example, if *R2d2* interacts with an intracellular structure as we propose, the same structure may guide it to the egg.⁵² Consistent with this idea, lagging chromosomes in the non-driving hybrid (Figure 2G) did not show biased retention in the egg (44.9% of $n = 49$ lagging chromosomes remained in the egg). Interestingly, univalent chromosomes lag and preferentially segregate to the polar body in *C. elegans*, implying species divergence in how oocytes handle anaphase lagging chromosomes.⁵⁴ When bivalents could be identified as either recombinant or non-recombinant (Figure 1B), we found that recombinant chromosomes (which compete in meiosis II) lag but eventually segregate equally in meiosis I. The mechanism underlying this equal segregation is unclear, but it is consistent with the previous observation that females homozygous for *R2d2* do not exhibit reduced fertility.³⁰ Bivalents in *R2d2* homozygous oocytes would be symmetric for *R2d2*, similar to recombinant bivalents in our experiment. Future work should seek to elucidate how

preferential segregation, and therefore aneuploidy, is avoided when homologous chromosomes both have the high-copy *R2d2* allele.

Recombination pattern and *R2d2* meiotic drive

Roughly three-quarters of metaphase II eggs from *R2d2* heterozygous mice harbored a crossover in between *R2d2* and the centromere (Figure S4A), indicating that *R2d2* has the opportunity to cheat more often in meiosis II. Metaphase II eggs from the non-driving hybrid also exhibited a high rate of such recombinant chromosomes (Figure S4B). If anaphase lagging is a more effective drive strategy in meiosis II, as suggested by our analyses of lagging chromosomes (Figures 2B–2D), then higher recombinant rates would be beneficial for *R2d2* to further increase its ability to drive. The maize knob domain cheats in meiosis II, and its location far from the centromere increases the chances to become a recombinant, allowing its cheating in meiosis II. Because *R2d2* is located in the middle of chromosome 2, which has uniform recombination distribution across the chromosome in female meiosis, it remains unclear why there are more recombinants.^{29,55} It would be an interesting future direction to pursue the underlying mechanism.

In conclusion, this work provides the first cell biological insights into how a non-centromeric selfish element can bias its transmission through female meiosis in animals. We would like to note that this study primarily used meiosis I oocytes due to technical difficulty in labeling the *R2d2* locus in anaphase II. Our anaphase lagging analyses (Figures 2C and 2D) imply that *R2d2* also lags in meiosis II and induces aneuploidy. Alternatively, *R2d2* may employ a different cheating strategy in meiosis II to achieve the extremely strong transmission bias.

Asymmetry in cell fate is a fundamental difference between female and male meiosis, which may have originated as a strategy for selfish meiotic drivers to increase their transmission by gamete killing.⁵⁶ Such strategies are well documented in male meiosis, and our findings indicate that they also persist in female meiosis, except that *R2d2* sabotages gametes that are products of different meiotic divisions rather than sisters from the same division.

STAR★METHODS

Detailed methods are provided in the online version of this paper and include the following:

- KEY RESOURCES TABLE
- RESOURCE AVAILABILITY
 - Lead contact
 - Materials availability
 - Data and code availability
- EXPERIMENTAL MODEL AND STUDY PARTICIPANT DETAILS
 - Mouse strains
- METHOD DETAILS
 - Mouse oocyte collection and culture
 - Oocyte microinjection
 - Oligopaint design methods
 - Immunostaining and Oligopaint FISH of oocytes and eggs
 - Oligopaint FISH of bone marrow cells
 - Microscopy and Image analysis
- QUANTIFICATION AND STATISTICAL ANALYSIS

SUPPLEMENTAL INFORMATION

Supplemental information can be found online at <https://doi.org/10.1016/j.cub.2024.07.001>.

ACKNOWLEDGMENTS

We thank Dr. Elissa P. Lei for the comments on the manuscript; the Cell and Developmental Biology Microscopy Core director, Dr. Andrea Stout, at the University of Pennsylvania for assistance with the super-resolution microscopy; Fernando Pardo-Manuel de Villena, the Akera lab, and the Lampson lab members for discussion; and our animal facilities for their particular care of our challenging mouse strains. This work is supported by the Intramural Programs of National Heart, Lung, and Blood Institute (1ZIAHL006249-01) (T.A.) and the Eunice Kennedy Shriver National Institute of Child Health and Human Development (1K99HD104851) (L.F.R.) at the National Institutes of Health (NIH) and the NIH grant R35GM122475 (M.A.L.).

AUTHOR CONTRIBUTIONS

Conceptualization, T.A. and M.A.L.; methodology, T.A., F.E.C., N.L.G., and L.F.R.; investigation, T.A., E.T., M.S., R.Z.W., F.E.C., D.M.Z.A.S., and N.L.G.; writing – original draft, F.E.C.; writing – review & editing, F.E.C., N.L.G., T.A., and M.A.L.; funding acquisition, T.A., and M.A.L.; resources, T.A. and M.A.L.; supervision, T.A. and M.A.L.

DECLARATION OF INTERESTS

The authors declare no competing interests.

Received: March 8, 2024

Revised: May 31, 2024

Accepted: July 1, 2024

Published: July 26, 2024

REFERENCES

- Clark, F.E., and Akera, T. (2021). Unravelling the mystery of female meiotic drive: where we are. *Open Biol.* *11*, 210074. <https://doi.org/10.1098/rsob.210074>.
- Chmátal, L., Schultz, R.M., Black, B.E., and Lampson, M.A. (2017). Cell Biology of Cheating—Transmission of Centromeres and Other Selfish Elements Through Asymmetric Meiosis. In *Progress in Molecular and Subcellular Biology* (Springer), pp. 377–396. https://doi.org/10.1007/978-3-319-58592-5_16.
- Pardo-Manuel de Villena, F., and Sapienza, C. (2001). Nonrandom segregation during meiosis: the unfairness of females. *Mamm. Genome* *12*, 331–339. <https://doi.org/10.1007/s003350040003>.
- Kruger, A.N., and Mueller, J.L. (2021). Mechanisms of meiotic drive in symmetric and asymmetric meiosis. *Cell. Mol. Life Sci.* *78*, 3205–3218. <https://doi.org/10.1007/s00018-020-03735-0>.
- Courret, C., Chang, C.-H., Wei, K.H.-C., Montchamp-Moreau, C., and Larracuente, A.M. (2019). Meiotic drive mechanisms: lessons from *Drosophila*. *Proc. Biol. Sci.* *286*, 20191430. <https://doi.org/10.1098/rspb.2019.1430>.
- McLaughlin, R.N., and Malik, H.S. (2017). Genetic conflicts: the usual suspects and beyond. *J. Exp. Biol.* *220*, 6–17. <https://doi.org/10.1242/jeb.148148>.
- Helleu, Q., Gérard, P.R., and Montchamp-Moreau, C. (2014). Sex chromosome drive. *Cold Spring Harb. Perspect. Biol.* *7*, a017616. <https://doi.org/10.1101/cshperspect.a017616>.
- Lindholm, A.K., Dyer, K.A., Firman, R.C., Fishman, L., Forstmeier, W., Holman, L., Johannesson, H., Knief, U., Kokko, H., Larracuente, A.M., et al. (2016). The Ecology and Evolutionary Dynamics of Meiotic Drive. *Trends Ecol. Evol.* *31*, 315–326. <https://doi.org/10.1016/j.tree.2016.02.001>.
- Finseth, F. (2023). Female meiotic drive in plants: mechanisms and dynamics. *Curr. Opin. Genet. Dev.* *82*, 102101. <https://doi.org/10.1016/j.gde.2023.102101>.
- Yoshida, K., and Kitano, J. (2012). The contribution of female meiotic drive to the evolution of neo-sex chromosomes. *Evolution* *66*, 3198–3208. <https://doi.org/10.1111/j.1558-5646.2012.01681.x>.
- Hanlon, S.L., and Hawley, R.S. (2023). B chromosomes reveal a female meiotic drive suppression system in *Drosophila melanogaster*. *Curr. Biol.* *33*, 2300–2306.e5. <https://doi.org/10.1016/j.cub.2023.04.028>.
- Eickbush, M.T., Young, J.M., and Zanders, S.E. (2019). Killer Meiotic Drive and Dynamic Evolution of the wtf Gene Family. *Mol. Biol. Evol.* *36*, 1201–1214. <https://doi.org/10.1093/molbev/msz052>.
- Zanders, S.E., and Unckless, R.L. (2019). Fertility Costs of Meiotic Drivers. *Curr. Biol.* *29*, R512–R520. <https://doi.org/10.1016/j.cub.2019.03.046>.
- Henikoff, S., Ahmad, K., and Malik, H.S. (2001). The centromere paradox: stable inheritance with rapidly evolving DNA. *Science* *293*, 1098–1102. <https://doi.org/10.1126/science.1062939>.
- Rosin, L.F., and Mellone, B.G. (2017). Centromeres Drive a Hard Bargain. *Trends Genet.* *33*, 101–117. <https://doi.org/10.1016/j.tig.2016.12.001>.
- Cheeseman, I.M., and Desai, A. (2008). Molecular architecture of the kinetochore-microtubule interface. *Nat. Rev. Mol. Cell Biol.* *9*, 33–46. <https://doi.org/10.1038/nrm2310>.
- Black, B.E., and Cleveland, D.W. (2011). Epigenetic centromere propagation and the nature of CENP-a nucleosomes. *Cell* *144*, 471–479. <https://doi.org/10.1016/j.cell.2011.02.002>.
- Foley, E.A., and Kapoor, T.M. (2013). Microtubule attachment and spindle assembly checkpoint signalling at the kinetochore. *Nat. Rev. Mol. Cell Biol.* *14*, 25–37. <https://doi.org/10.1038/nrm3494>.
- Das, A., Smoak, E.M., Linares-Saldana, R., Lampson, M.A., and Black, B.E. (2017). Centromere inheritance through the germline. *Chromosoma* *126*, 595–604. <https://doi.org/10.1007/s00412-017-0640-y>.
- Iwata-Otsubo, A., Dawicki-McKenna, J.M., Akera, T., Falk, S.J., Chmátal, L., Yang, K., Sullivan, B.A., Schultz, R.M., Lampson, M.A., and Black, B.E. (2017). Expanded Satellite Repeats Amplify a Discrete CENP-A Nucleosome Assembly Site on Chromosomes that Drive in Female Meiosis. *Curr. Biol.* *27*, 2365–2373.e8. <https://doi.org/10.1016/j.cub.2017.06.069>.
- Wu, T., Lane, S.I.R., Morgan, S.L., and Jones, K.T. (2018). Spindle tubulin and MTOC asymmetries may explain meiotic drive in oocytes. *Nat. Commun.* *9*, 2952. <https://doi.org/10.1038/s41467-018-05338-7>.
- Fishman, L., and Saunders, A. (2008). Centromere-associated female meiotic drive entails male fitness costs in monkeyflowers. *Science* *322*, 1559–1562. <https://doi.org/10.1126/science.1161406>.
- Akera, T., Chmátal, L., Trimm, E., Yang, K., Aonbangkhen, C., Chenoweth, D.M., Janke, C., Schultz, R.M., and Lampson, M.A. (2017). Spindle asymmetry drives non-Mendelian chromosome segregation. *Science* *358*, 668–672. <https://doi.org/10.1126/science.aan0092>.
- Akera, T., Trimm, E., and Lampson, M.A. (2019). Molecular Strategies of Meiotic Cheating by Selfish Centromeres. *Cell* *178*, 1132–1144.e10. <https://doi.org/10.1016/j.cell.2019.07.001>.
- Kumon, T., Ma, J., Akins, R.B., Stefanik, D., Nordgren, C.E., Kim, J., Levine, M.T., and Lampson, M.A. (2021). Parallel pathways for recruiting effector proteins determine centromere drive and suppression. *Cell* *184*, 4904–4918.e11. <https://doi.org/10.1016/j.cell.2021.07.037>.
- Silva, D.M., and Akera, T. (2023). Meiotic drive of noncentromeric loci in mammalian meiosis II eggs. *Curr. Opin. Genet. Dev.* *81*, 102082. <https://doi.org/10.1016/j.gde.2023.102082>.
- Dawe, R.K., Lowry, E.G., Gent, J.I., Stitzer, M.C., Swentowsky, K.W., Higgins, D.M., Ross-Ibarra, J., Wallace, J.G., Kanizay, L.B., Alabady, M., et al. (2018). A Kinesin-14 Motor Activates Neocentromeres to Promote Meiotic Drive in Maize. *Cell* *173*, 839–850.e18. <https://doi.org/10.1016/j.cell.2018.03.009>.

28. Swentowsky, K.W., Gent, J.I., Lowry, E.G., Schubert, V., Ran, X., Tseng, K.-F., Harkess, A.E., Qiu, W., and Dawe, R.K. (2020). Distinct kinesin motors drive two types of maize neocentromeres. *Genes Dev.* **34**, 1239–1251. <https://doi.org/10.1101/gad.340679.120>.
29. Didion, J.P., Morgan, A.P., Clayshulte, A.M.-F., McMullan, R.C., Yadgary, L., Petkov, P.M., Bell, T.A., Gatti, D.M., Crowley, J.J., Hua, K., et al. (2015). A multi-megabase copy number gain causes maternal transmission ratio distortion on mouse chromosome 2. *PLoS Genet.* **11**, e1004850. <https://doi.org/10.1371/journal.pgen.1004850>.
30. Morgan, A.P., Holt, J.M., McMullan, R.C., Bell, T.A., Clayshulte, A.M.F., Didion, J.P., Yadgary, L., Thybert, D., Odom, D.T., Flicek, P., et al. (2016). The Evolutionary Fates of a Large Segmental Duplication in Mouse. *Genetics* **204**, 267–285. <https://doi.org/10.1534/genetics.116.191007>.
31. Didion, J.P., Morgan, A.P., Yadgary, L., Bell, T.A., McMullan, R.C., Ortiz de Solorzano, L., Britton-Davidian, J., Bult, C.J., Campbell, K.J., Castiglia, R., et al. (2016). R2d2 Drives Selfish Sweeps in the House Mouse. *Mol. Biol. Evol.* **33**, 1381–1395. <https://doi.org/10.1093/molbev/msw036>.
32. Anton, T., Bultmann, S., Leonhardt, H., and Markaki, Y. (2014). Visualization of specific DNA sequences in living mouse embryonic stem cells with a programmable fluorescent CRISPR/Cas system. *Nucleus* **5**, 163–172. <https://doi.org/10.4161/nucl.28488>.
33. Beliveau, B.J., Joyce, E.F., Apostolopoulos, N., Yilmaz, F., Fonseka, C.Y., McCole, R.B., Chang, Y., Li, J.B., Senaratne, T.N., Williams, B.R., et al. (2012). Versatile design and synthesis platform for visualizing genomes with Oligopaint FISH probes. *Proc. Natl. Acad. Sci. USA* **109**, 21301–21306. <https://doi.org/10.1073/pnas.1213818110>.
34. Dudka, D., and Lampson, M.A. (2022). Centromere drive: model systems and experimental progress. *Chromosome Res.* **30**, 187–203. <https://doi.org/10.1007/s10577-022-09696-3>.
35. Agulnik, S.I., Agulnik, A.I., and Ruvinsky, A.O. (1990). Meiotic drive in female mice heterozygous for the HSR inserts on chromosome 1. *Genet. Res.* **55**, 97–100. <https://doi.org/10.1017/s0016672300025325>.
36. Li, R., and Albertini, D.F. (2013). The road to maturation: somatic cell interaction and self-organization of the mammalian oocyte. *Nat. Rev. Mol. Cell Biol.* **14**, 141–152. <https://doi.org/10.1038/nrm3531>.
37. Dehapiot, B., Clément, R., Bourdais, A., Carrière, V., Huet, S., and Halet, G. (2021). RhoA- and Cdc42-induced antagonistic forces underlie symmetry breaking and spindle rotation in mouse oocytes. *PLoS Biol.* **19**, e3001376. <https://doi.org/10.1371/journal.pbio.3001376>.
38. Wang, H., Li, Y., Yang, J., Duan, X., Kalab, P., Sun, S.X., and Li, R. (2020). Symmetry breaking in hydrodynamic forces drives meiotic spindle rotation in mammalian oocytes. *Sci. Adv.* **6**, eaaz5004. <https://doi.org/10.1126/sciadv.aaz5004>.
39. Dyban, A.P., and Baranov, V.S. (1987). *Cytogenetics of Mammalian Embryonic Development* (Oxford University Press).
40. Torres, E.M., Williams, B.R., and Amon, A. (2008). Aneuploidy: cells losing their balance. *Genetics* **179**, 737–746. <https://doi.org/10.1534/genetics.108.090878>.
41. Chmátal, L., Gabriel, S.I., Mitsainas, G.P., Martínez-Vargas, J., Ventura, J., Searle, J.B., Schultz, R.M., and Lampson, M.A. (2014). Centromere strength provides the cell biological basis for meiotic drive and karyotype evolution in mice. *Curr. Biol.* **24**, 2295–2300. <https://doi.org/10.1016/j.cub.2014.08.017>.
42. Pardo-Manuel de Villena, F., and Sapienza, C. (2001). Female Meiosis Drives Karyotypic Evolution in Mammals. *Genetics* **159**, 1179–1189. <https://doi.org/10.1093/genetics/159.3.1179>.
43. Zanders, S.E., Eickbush, M.T., Yu, J.S., Kang, J.-W., Fowler, K.R., Smith, G.R., and Malik, H.S. (2014). Genome rearrangements and pervasive meiotic drive cause hybrid infertility in fission yeast. *eLife* **3**, e02630. <https://doi.org/10.7554/eLife.02630>.
44. Larracuent, A.M., and Presgraves, D.C. (2012). The selfish Segregation Distorter gene complex of *Drosophila melanogaster*. *Genetics* **192**, 33–53. <https://doi.org/10.1534/genetics.112.141390>.
45. Grognet, P., Lalucque, H., Malagnac, F., and Silar, P. (2014). Genes that bias Mendelian segregation. *PLoS Genet.* **10**, e1004387. <https://doi.org/10.1371/journal.pgen.1004387>.
46. Presgraves D. (2009) In: T.R. Birkhead, D.J. Hosken, S. Pitnick, eds., pp. 471–506. <https://doi.org/10.1016/B978-0-12-372568-4.00012-4>.
47. Chesler, E.J., Gatti, D.M., Morgan, A.P., Strobel, M., Trepanier, L., Oberbeck, D., McWeeney, S., Hitzemann, R., Ferris, M., McMullan, R., et al. (2016). Diversity Outbred Mice at 21: Maintaining Allelic Variation in the Face of Selection. *G3 (Bethesda)* **6**, 3893–3902. <https://doi.org/10.1534/g3.116.035527>.
48. Ruban, A., Schmutzer, T., Wu, D.D., Fuchs, J., Boudichevskaia, A., Rubtsova, M., Pistrick, K., Melzer, M., Himmelbach, A., Schubert, V., et al. (2020). Supernumerary B chromosomes of *Aegilops speltoides* undergo precise elimination in roots early in embryo development. *Nat. Commun.* **11**, 2764. <https://doi.org/10.1038/s41467-020-16594-x>.
49. Wu, D.D., Ruban, A., Fuchs, J., Macas, J., Novák, P., Vaio, M., Zhou, Y.H., and Houben, A. (2019). Nondisjunction and unequal spindle organization accompany the drive of *Aegilops speltoides* B chromosomes. *New Phytol.* **223**, 1340–1352. <https://doi.org/10.1111/nph.15875>.
50. Banaei-Moghaddam, A.M., Schubert, V., Kumke, K., Weiß, O., Klemme, S., Nagaki, K., Macas, J., González-Sánchez, M., Heredia, V., Gómez-Revilla, D., et al. (2012). Nondisjunction in Favor of a Chromosome: The Mechanism of Rye B Chromosome Drive during Pollen Mitosis. *Plant Cell* **24**, 4124–4134. <https://doi.org/10.1105/tpc.112.105270>.
51. Mogessie, B., and Schuh, M. (2017). Actin protects mammalian eggs against chromosome segregation errors. *Science* **357**, eaal1647. <https://doi.org/10.1126/science.aal1647>.
52. Dalton, C.M., and Carroll, J. (2013). Biased inheritance of mitochondria during asymmetric cell division in the mouse oocyte. *J. Cell Sci.* **126**, 2955–2964. <https://doi.org/10.1242/jcs.128744>.
53. Ferrandiz, N., Downie, L., Starling, G.P., and Royle, S.J. (2022). Endomembranes promote chromosome missegregation by ensheathing misaligned chromosomes. *J. Cell Biol.* **221**, e202203021. <https://doi.org/10.1083/jcb.202203021>.
54. Cortes, D.B., McNally, K.L., Mains, P.E., and McNally, F.J. (2015). The asymmetry of female meiosis reduces the frequency of inheritance of unpaired chromosomes. *eLife* **4**, e06056. <https://doi.org/10.7554/eLife.06056>.
55. Liu, E.Y., Morgan, A.P., Chesler, E.J., Wang, W., Churchill, G.A., and Pardo-Manuel de Villena, F. (2014). High-Resolution Sex-Specific Linkage Maps of the Mouse Reveal Polarized Distribution of Crossovers in Male Germline. *Genetics* **197**, 91–106. <https://doi.org/10.1534/genetics.114.161653>.
56. Malik, H.S., and Henikoff, S. (2009). Major evolutionary transitions in centromere complexity. *Cell* **138**, 1067–1082. <https://doi.org/10.1016/j.cell.2009.08.036>.
57. Miyanari, Y., Ziegler-Birling, C., and Torres-Padilla, M.-E. (2013). Live visualization of chromatin dynamics with fluorescent TALEs. *Nat. Struct. Mol. Biol.* **20**, 1321–1324. <https://doi.org/10.1038/nsmb.2680>.
58. El Yakoubi, W., and Akera, T. (2023). Condensin dysfunction is a reproductive isolating barrier in mice. *Nature* **623**, 347–355. <https://doi.org/10.1038/s41586-023-06700-6>.
59. Beliveau, B.J., Kishi, J.Y., Nir, G., Sasaki, H.M., Saka, S.K., Nguyen, S.C., Wu, C.T., and Yin, P. (2018). OligoMiner provides a rapid, flexible environment for the design of genome-scale oligonucleotide in situ hybridization probes. *Proc. Natl. Acad. Sci. USA* **115**, E2183–E2192. <https://doi.org/10.1073/pnas.1714530115>.
60. Rosin, L.F., Jr., Gil, J., Drinnenberg, I.A., and Lei, E.P. (2021). Oligopaint DNA FISH reveals telomere-based meiotic pairing dynamics in the

- silkworm, *Bombyx mori*. *PLoS Genet.* 17, e1009700. <https://doi.org/10.1371/journal.pgen.1009700>.
61. Langmead, B., and Salzberg, S.L. (2012). Fast gapped-read alignment with Bowtie 2. *Nat. Methods* 9, 357–359. <https://doi.org/10.1038/nmeth.1923>.
62. Schindelin, J., Arganda-Carreras, I., Frise, E., Kaynig, V., Longair, M., Pietzsch, T., Preibisch, S., Rueden, C., Saalfeld, S., Schmid, B., et al. (2012). Fiji: an open-source platform for biological-image analysis. *Nat. Methods* 9, 676–682. <https://doi.org/10.1038/nmeth.2019>.
63. Schneider, C.A., Rasband, W.S., and Eliceiri, K.W. (2012). NIH Image to ImageJ: 25 years of image analysis. *Nat. Methods* 9, 671–675. <https://doi.org/10.1038/nmeth.2089>.
64. Stein, P., and Schindler, K. (2011). Mouse oocyte microinjection, maturation and ploidy assessment. *J. Vis. Exp.* 53, 2851. <https://doi.org/10.3791/2851>.

STAR★METHODS

KEY RESOURCES TABLE

REAGENT or RESOURCE	SOURCE	IDENTIFIER
Antibodies		
Goat anti-GFP antibody conjugated with DyLight488	Rockland	Cat# 600-141-215; RRID: AB_1961516
Chemicals, peptides, and recombinant proteins		
M2 media	Sigma-Aldrich	M7167
M16 media	Millipore	M7292
Paraffin oil	Nacalai	NC1506764
Reversine	Sigma-Aldrich	R39-4-1MG
CARD HyperOva	Cosmo Bio USA	KYD-010-EX-X5
hCG	Sigma-Aldrich	C1063
Milrinone	Sigma-Aldrich	M4659
T7 mMessage mMachine kit	Ambion	AM1340
MEGAclear Transcription Clean-up kit	Thermo Fisher Scientific	AM1908
dCas9-EGFP protein	Novateinbio	PR-137213G
GeneArt Precision gRNA Synthesis kit	Thermo Fisher Scientific	A29377
Acidic Tyrode's Solution	EmbryoMax	MR-004-D
Poly-L-lysine	Sigma-Aldrich	P8920-100ML
Prolong Diamond Antifade Mountant	Invitrogen	P36966
Paraformaldehyde	Thermo Fisher Scientific	28908
Experimental models: Organisms/strains		
Mouse: NSA (CF1)	Envigo	033
Mouse: C57BL/6J	Jackson Laboratory	000664
Mouse: BXD19/TyJ	Jackson Laboratory	000010
Mouse: PWD/PhJ	Jackson Laboratory	004660
Mouse: WSB/EiJ	Jackson Laboratory	001145
Mouse: A/J	Jackson Laboratory	000646
Oligonucleotides		
gRNA	This paper	See Data S1A
Oligopaints (primary FISH probes)	This paper	See Data S1B–S1D
Secondary FISH probes with fluorophores (AlexF488, ATTO565, AlexF647)	Integrated DNA Technologies	Custom
Recombinant DNA		
H2B-mCherry	Akera et al. ²³	N/A
TALE-mClover-3x Halo	El Yakoubi and Akera ⁵⁸	N/A
Software and algorithms		
Oligominer pipeline	Beliveau et al. ³³ ; Beliveau et al. ⁵⁹ ; Rosin et al. ⁶⁰	N/A
Bowtie2	Langmead and Salzberg ⁶¹	N/A
Fiji/ImageJ	Schindelin et al. ⁶² ; Schneider et al. ⁶³	https://fiji.sc/
GraphPad Prism	GraphPad	http://www.graphpad.com/
Other		
Plastic pipette tip	Cooper Surgical Inc.	MXL3-75, MXL3-100, MXL3-125

RESOURCE AVAILABILITY

Lead contact

Further information and requests for resources and reagents should be directed to and will be fulfilled by the lead contact, Takashi Akera (takashi.akera@nih.gov).

Materials availability

This study did not generate new unique reagents. The sequence of gRNA and oligos used for dCas9 and oligopaint labeling, respectively, are provided in the [Data S1](#). Resources and reagents are available upon reasonable request.

Data and code availability

- All data reported in this paper will be shared by the [lead contact](#) upon request.
- This paper does not report original code.
- Any additional information required to reanalyze the data reported in this paper is available from the [lead contact](#) upon request.

EXPERIMENTAL MODEL AND STUDY PARTICIPANT DETAILS

Mouse strains

Mouse strains were purchased from Envigo (NSA, stock# 033 corresponds to CF1, *Mus musculus domesticus*), and from Jackson Laboratory (C57BL/6J, stock# 000664, *Mus musculus domesticus*, BXD19/TyJ, stock# 000010, *Mus musculus domesticus*, PWD/PhJ, Stock# 004660, *Mus musculus musculus*, WSB/EiJ, stock# 001145, *Mus musculus domesticus*, A/J, stock# 000646, *Mus musculus domesticus*). Strains CF1, C57BL/6J, BXD19/TyJ, A/J, and PWD/PhJ do not have high-copy *R2d2* repeats. WSB/EiJ has 33 copies of the *R2d2* monomer. Reciprocal crosses were used when crossing WSB/EiJ to other strains; however, the majority of F1 females used resulted from crosses where the sire was WSB/EiJ, as it is technically challenging to cross female WSB/EiJ with other strains. F1 females from WSB/EiJ crossed to C57BL/6J or BXD19/TyJ show over 90% transmission ratio distortion of the high-copy *R2d2* repeats (Didion et al.²⁹; F. Pardo-Manuel de Villena, personal communication), and we also confirmed that these genetic backgrounds have similar impacts on anaphase lagging in *R2d2* heterozygous oocytes ([Figure S2](#)). Mice were housed in an animal facility at room temperature, 30–70% humidity, and with a ventilated rack system. Mice were exposed to a 12 hr light/dark cycle year-round. Individuals used in experiments could be sisters or unrelated and ranged in age from 6 weeks to 6 months. Mice were euthanized with CO₂ followed by cervical dislocation prior to dissection of the ovaries or ampulla. All animal experiments were approved by the Animal Care and Use Committee (National Institutes of Health Animal Study Proposal#: H-0327) and were consistent with the National Institutes of Health guidelines.

METHOD DETAILS

Mouse oocyte collection and culture

All manipulation of oocytes or eggs was performed with a mouth-operated plastic pipette with either a 75, 100, or 125 μ m diameter pipette tip (Cooper Surgical, Inc., Cat# MXL3-75, MXL3-100, or MXL3-125, respectively). For *in vitro* oocyte culture, germinal vesicle-intact oocytes were collected from 6 week to 6 month-old female mice in M2 media (Sigma-Aldrich, Cat# M7167).⁶⁴ Oocytes were then kept in a 60 x15 mm polystyrene petri dish (Falcon, Cat# 351007) in either M2 media, covered with paraffin oil (Nacalai, Cat# NC1506764) and incubated at 37°C in a humidified atmosphere of 0% CO₂ in air, or transferred to M16 media (Millipore, Cat# M7292), covered with paraffin oil, and incubated at 37°C in a humidified atmosphere of 5% CO₂ in air. Both incubation environments were suitable, however, M16 media and an atmosphere containing 5% CO₂ in air resulted in slightly better cell viability under longer incubations. Oocytes were matured for variable times according to each assay. For analysis of metaphase I oocytes, cells were matured for 7 hr. For metaphase II eggs, cells were matured for 16 hr. For metaphase II eggs after the early onset of anaphase I by Reversine, cells were matured for 5 hr, transferred to M2 or M16 media with 0.5 μ M Reversine (Sigma-Aldrich, Cat# R39-4-1MG), and matured for an additional 11 hr. To visualize chromosomes, 50 nM sirDNA (Cytoskeleton, Inc., Cat# CY-SC007) was added to the media two hours prior to the live imaging. To collect *in vivo*-ovulated oocytes, female mice were injected with 0.1 ml CARD HyperOva (Cosmo Bio USA, Cat# KYD-010-EX-X5), then 5 IU of hCG (Sigma-Aldrich, Cat# C1063) 48 hr later, and euthanized 17 hr after the injection to dissect out ampulla. *In vivo*-ovulated metaphase II eggs were collected from the ampulla in M2 media, then transferred to M16 media, covered with paraffin oil in a 60 x15 mm polystyrene petri dish, and incubated at 37°C in a humidified atmosphere of 5% CO₂ in air for 1 hr.

Oocyte microinjection

GV-intact oocytes were microinjected with \sim 5 μ l of cRNAs or proteins in M2 containing 5 μ M milrinone (Sigma-Aldrich, Cat# M4659), using a micromanipulator TransferMan 4r and FemtoJet 4i (Eppendorf). Following the microinjection, oocytes were maintained at prophase I in M16 supplemented with 5 μ M milrinone overnight to allow protein expression. cRNAs used for microinjections were

MajSat (TALE construct that recognizes major satellite repeats fused to mClover⁵⁷ and 3 tandem Halo tag at the C terminus) at 1500 ng/ul and *H2B-mCherry* (human histone H2B with mCherry at the C terminus) at 100 ng/ul. cRNAs were synthesized using the T7 mMessage mMachine Kit (Ambion, Cat# AM1340) and purified using the MEGAClear Kit (Thermo Fisher Scientific, Cat# AM1908). The dCas9-EGFP-gRNA complex that targets the *R2d2* sequence was assembled *in vitro* by mixing 5 uM of dCas9-EGFP protein (Novateinbio, Cat# PR-137213G) with 5 uM of the gRNA pool for *R2d2* (see below) in the reaction buffer (2 mM HEPES, 10 mM NaCl, 5 mM MgCl₂, 10 μM EDTA, pH 6.5) and incubating at room temperature for 10 min. The dCas9 complex was subsequently mixed with the H2B-mCherry cRNA and used for microinjection. The gRNA pool is a mixture of 56 gRNA that have complementary sequences to the published *R2d2* sequence.³⁰ gRNAs were synthesized using the GeneArt Precision gRNA Synthesis kit (Thermo Fisher Scientific, Cat# A29377). We were able to visualize the *R2d2* locus with 56 gRNA but not with 20 or 40 gRNA (data not shown). The list of primer sets that were used to produce each gRNA are provided in [Data S1A](#).

Oligopaint design methods

Oligopaints were designed (see [Figure S1A](#) for schematic) using a modified version of the Oligominer pipeline as previously described and the mm9 genome assembly.^{33,59,60} For the *R2d2* locus probes, the *R2d2* sequence was obtained from the Morgan et al. paper.³⁰ Bowtie2 was used to find oligos that uniquely mapped to the *R2d2* locus using the –very-sensitive-local alignment parameters.⁶¹ The final probe density was designed to be about 0.5 probes per kb, and oligos contained 42–80 bp of homology. The specificity of these oligopaints for *R2d2*, and not *R2d1*, is demonstrated in the labeling of heterozygous cells ([Figures S1B](#) and [S1C](#)). For Oligopaints labeling the 7 Mb domain on chromosome 2, probes were at a density of 2 probes per kb with 80 bp homology. For Oligopaints labeling the middle of chromosome 1, the mm39 genome assembly was used, and probes were at a density of ~3 probes per kb with 70 bp homology. A complete list of oligo loci and sequences can be found in [Data S1B–S1D](#).

Immunostaining and Oligopaint FISH of oocytes and eggs

Oocytes and eggs matured to the appropriate stage (and with the zona pellucida removed by Acidic Tyrode's Solution (EmbryoMax, Cat# MR-004-D) for the FISH assay) were fixed in freshly prepared 2% paraformaldehyde (Thermo Scientific, Cat# 28908) in 1x PBS (Quality Biological, Cat# 119-069-101) for 20 min at room temperature (RT). Fixed cells were then washed in the blocking solution (0.3% BSA (Fisher Bioreagents, Cat# BP1600-100) and 0.01% Tween (Thermo Scientific, Cat# 9005-64-5) in 1x PBS). Cells were then permeabilized in 1x PBS with 0.1% Triton X-100 (Millipore, Cat# TX1568-1) for 15 min at RT, then placed in the blocking solution.

For immunostaining assays, the cells were then incubated for 1 hr at RT or overnight at 4°C in the blocking solution with the goat anti-GFP antibody conjugated with Dylight488 (1:100, Rockland, Cat# 600-141-215). After washing three times (10 min each) in the blocking solution, cells were then mounted on microscope slides with Antifade Mounting Medium with DAPI (Vector Laboratories, Cat# H-1200) and then sealed with L.A. Colors top coat rapid dry clear polish (Electron Microscopy Sciences, Cat# 72180).

For FISH assays, demonstrated in [Figure S1C](#), the cells were mounted on microscope slides (Fisher Scientific, Cat# 12-544-3) by transferring them in a small drop of blocking solution to the surface of a 0.01% poly-L-lysine (Sigma-Aldrich, Cat# P8920-100ML) coated slide. Following a 2 min incubation, the cells were washed (on the slide) with 1x PBS four times for 10 min each. Cells were then fixed a second time with 4% paraformaldehyde, 0.1% Triton X-100 in 1x PBS for 20 min at RT. The microscope slides were then washed (in Coplin jars) in 1x PBS three times for 5 min at RT, in 0.7% Triton X-100 / 0.1 M HCl (LabChem, Cat# LC153004) for 10 min at RT, in 2x SSCT (0.1% Tween-20 in 2x SSC (Promega, Cat# V4261)) for 5 min at RT, in 50% (v/v) formamide (Fisher BioReagents, Cat# BP227-500) in 2x SSCT for 5 min at RT, in 50% formamide in 2x SSCT for 2.5 min at 85°C, and in 50% formamide in 2x SSCT for 20 min at 60°C. Slides were then cooled at RT for 10 min and a 22 mm round coverslip (Fisher Scientific, Cat# 12545101) with a primary Oligopaint mix was mounted to the slides and sealed with rubber cement (Elmer's, Cat# E904). The primary Oligopaint mix was composed of 100 pmol of each Oligopaint, 1.5 μl of 25 μM dNTPs (New England BioLabs, Cat# N0446S), 1 μl molecular grade H₂O, 12.5 μl formamide, 4 μl PVSA (Sigma-Aldrich, Cat# 278424), 1 μl RNase A (VWR Life Science, Cat# E866-5ML), 6.25 μl DNA hybridization buffer (4 g Dextran sulfate sodium salt (Sigma-Aldrich, Cat# D8906-100G), 40 μl Tween, 4 ml 20x SSC, PVSA up to 10 ml), per reaction. Once the rubber cement had completely dried, the microscope slide was heated to 85°C on a metal block for 2.5 min, and immediately transferred to a 37°C humidified chamber for an overnight incubation. The following day, the cover slips were removed and slides were washed (in coplin jars) in 2x SSCT for 15 min at 60°C, in 2x SSCT for 15 min at RT, and in 0.2x SSC for 10 min at RT. A 22 mm round coverslip with a secondary Oligopaint mix was mounted to the slides and sealed with rubber cement. The secondary Oligopaint mix was composed of 10 pmol of each secondary oligo (IDT, custom synthesized), 6.25 μl DNA hybridization buffer, 12.5 μl formamide, and H₂O up to 25 μl, per reaction. Slides were then transferred to a 37°C humidified chamber for 2 hr. Following this, the cover slips were removed and slides were washed in 2x SSCT for 15 min at 60°C, in 2x SSCT for 15 min at RT, and in 0.2x SSC for 10 min at RT. A square 22 mm x 22 mm #1.5 coverslip (VWR, Cat# 16004-302) with a drop of Prolong Diamond Antifade Mountant with DAPI (Invitrogen, Cat# P36966) was mounted to the slides. Slides were allowed to set for either 24 hr at RT or 72 hr at 4°C, and then sealed with clear polish.

Oligopaint FISH of bone marrow cells

To prepare metaphase chromosome spreads in [Figure S1B](#), bone marrow from femurs and tibias was flushed out into 2.85 ml of M2 media at 37°C using a 1 cc tuberculin syringe and 23g needle. Bone marrow was then broken up and 150 μl of 0.5% colchicine (Sigma-Aldrich, Cat# C9754-500MG) was added. The suspension was incubated for 10 min at 37°C, and the media was removed by centrifugation at 400 × g for 5 min and removing the supernatant. The pellet was resuspended in 1.5 ml 0.56% KCl solution

and incubated for 20 min at 37°C. The suspension was then centrifuged as above, and the supernatant was removed. Cells were fixed with three subsequent rounds of standard washing with methanol/acetic acid (Macron Fine Chemicals, Cat# MK-3016-16 and MK-V193-45) (3/1) fixative solution. The final pellet was diluted in methanol/acetic acid solution and dropped on a clean microscopy slide covered with a steam layer and air dried for two days. To perform Oligopaint FISH, the slides were washed in 1x PBS for 5 min at RT and incubated in 0.005% Pepsin (Sigma-Aldrich, Cat# P7012-250MG) in 0.01 N HCl solution for 10 min at 37°C. The slides were then washed in 1x PBS at RT and fixed in 1% paraformaldehyde in 1x PBS for 10 min at RT and washed in 1x PBS for 5 min at RT. The slides were dehydrated in a series of graded alcohols (70%, 90%, and 100%), air dried, and the primary Oligopaint mix was mounted to the slides and sealed with rubber cement (Elmer's, Cat# E904). Subsequent steps were performed as for Oligopaint FISH of oocytes and eggs.

Microscopy and Image analysis

Fixed oocytes, eggs, and bone marrow cells were imaged with a microscope (Eclipse Ti; Nikon) equipped with 100x / 1.40 NA oil-immersion objective lens, CSU-W1 spinning disk confocal scanner (Yokogawa), ORCA Fusion Digital CMOS camera (Hamamatsu Photonics), and 405, 488, 561 and 640 nm laser lines controlled by the NIS-Elements imaging software (Nikon). Confocal images were acquired as Z-stacks at 0.3 μ m intervals. For live imaging, oocytes were placed into 3 μ l drops of M2 covered with paraffin oil in a glass-bottom tissue culture dish (fluoroDish, Cat# FD35-100) in a stage top incubator (Tokai Hit) to maintain 37°C. Time-lapse images were collected with a microscope (Eclipse Ti2-E; Nikon) equipped with the 20x / 0.75 NA objective and 60x / 1.40 NA oil-immersion objective, CSU-W1 spinning disk confocal scanner (Yokogawa), ORCA Fusion Digital CMOS camera (Hamamatsu Photonics), and 405, 488, 561 and 640 nm laser lines controlled by the NIS-Elements imaging software (Nikon). For the biased orientation assay in [Figure 1D](#), images of one of the experiments were taken with a microscope (Olympus IX71) equipped with 100x / 1.40 NA oil-immersion objective lens, Visitech VT iSIM scan head, ORCA Quest qCMOS camera (Hamamatsu Photonics), and 405, 442, 488, 514, 561, 640 nm laser lines controlled by MetaMorph acquisition software. Images are displayed as maximum intensity Z-projections. Due to the weak dCas9-EGFP signals during live-imaging experiments ([Figures 3](#), [S3A](#), and [S3B](#)), we used the Denoise.ai software (Nikon) to reduce noise and follow the *R2d2* locus better in anaphase I. Fiji/ImageJ (NIH) was used to analyze all the images.^{62,63}

QUANTIFICATION AND STATISTICAL ANALYSIS

Data points were pooled from two to six independent experiments. Data analysis was performed using Microsoft Excel and GraphPad Prism 10. Scattered plots, bar graphs, and line graphs were created with GraphPad Prism 10. Unpaired two-tailed t-test ([Figures 2D](#) and [S2](#)), chi-square test for goodness of fit for deviations from the expected 50:50 ratio ([Figures 2B](#), [2C](#), and [S4](#)), and chi-square test of independence ([Figures 3C](#), [4A](#), and [S3B](#)) were used for statistical analyses, and the actual *P* values are shown in each figure or figure legend.